Molecular modeling of polycarbonate materials: Glass transition and mechanical properties

Karol Palczynski*
Institut für Weiche Materie und Funktionale Materialien, Helmholtz-Zentrum Berlin für Materialien und Energie, Hahn-Meitner Platz 1, 14109 Berlin, Germany

Andreas Wilke and Manfred Paeschke
Bundesdruckerei GmbH, Kommandantenstraße 18, 10969 Berlin, Germany

Joachim Dzubiella†
Institut für Physik, Humboldt-Universität zu Berlin, Newtonstraße 15, 12489 Berlin, Germany
and Institut für Weiche Materie und Funktionale Materialien, Helmholtz-Zentrum Berlin für Materialien und Energie, Hahn-Meitner Platz 1, 14109 Berlin, Germany

(Received 17 May 2017; published 27 September 2017)

Linking the experimentally accessible macroscopic properties of thermoplastic polymers to their microscopic static and dynamic properties is a key requirement for targeted material design. Classical molecular dynamics simulations enable us to study the structural and dynamic behavior of molecules on microscopic scales, and statistical physics provides a framework for relating these properties to the macroscopic properties. We take a first step toward creating an automated workflow for the theoretical prediction of thermoplastic material properties by developing an expeditious method for parameterizing a simple yet surprisingly powerful coarse-grained bisphenol-A polycarbonate model which goes beyond previous coarse-grained models and successfully reproduces the thermal expansion behavior, the glass transition temperature as a function of the molecular weight, and several elastic properties.

DOI: 10.1103/PhysRevMaterials.1.043804

I. INTRODUCTION

Bisphenol-A polycarbonate (PC) is a thermoplastic of high thermal stability and toughness, very suitable for engineering and durable goods applications [1]. One key aspect in terms of manufacturing (processing temperature) and applications (thermal stability) is the glass transition temperature. The mechanism of the glass transition and all its contributing factors, such as the molecular weight, polydispersity, entanglement behavior, effects of additives, or functionalization, are not fully understood on a molecular level to this day. The earliest microscopic models of the glass transition are still used today [2–6].

Experimentally, on a macroscopic level, the glass transition temperature and other thermal properties of PC such as the heat capacity, volume expansion, and viscoelastic properties have been investigated already [7–11]. These studies have been followed by x-ray diffraction measurements of the molecular ordering and intrinsic chain dynamics in the amorphous and crystalline states of PC, providing details about the angles between chain segments and chain segment mobility [12–14]. Consequently, the first all-atom simulation studies aimed at recreating single PC chain structures and aspects of intrachain mobility on very short time scales such as the rotation frequencies of individual chain segments [15]. However, for a long time, rigorous theoretical investigations of structural and dynamic PC properties have been beyond the capacity of available computers. Even to this day, because of the complexity of PC, molecular dynamics (MD) models have to rely on major simplifications in order to study the dynamic behavior of PC. First efforts to create a force field with all degrees of freedom (DOF) on the atomistic level have been published by Sun *et al.* [16], based on *ab initio* calculations and some scaling to fit intrachain structures from experimental data. Subsequently, several other all-atom force fields of PC have been developed, quantitatively exploring rotational diffusion [14] or even attempting to reproduce stress-strain behavior [17].

It became increasingly clear, that in order to link the macroscopic properties of PC to its microscopic properties using molecular simulations, many atomistic DOF had to be sacrificed by means of coarse graining in favor of larger length and time scales [18,19]. To varying degree of detail, depending on the specific material properties of interest, entire segments of an atomistic model can be substituted by single geometrical structures, typically beads. Effective interactions between the beads replace the detailed chemistry of the atomistic segments in a way that retains the statistical collective behavior of the chain segments. This requires defining two types of interactions, intramolecular (or bonded) interactions which reproduce the statistical behavior of the bond lengths and angles inside a polymeric chain, and intermolecular interactions which describe the energies between beads that are not directly correlated with each other through the intramolecular (or nonbonded) interactions, such as beads that belong to separate chains. While suitable intramolecular interactions are straightforward to determine, the systematic way of parameterizing the intermolecular interactions, called iterative Boltzmann inversion, is computationally very expensive for a molecule as complex as PC [20]. It is so difficult, in fact, that up until recently the typical way of treating nonbonded interactions of PC was by making them purely repulsive.

*karol.palczynski@helmholtz-berlin.de
†joachim.dzubiella@helmholtz-berlin.de

The first attempts of this kind already attained reasonable agreement with experimental diffusion coefficients of short chains (∼10–20 monomers) in PC melts at temperatures $T > 500$ K [21,22]. At these temperatures, the thermal energy $k_B T$ is typically higher than the attraction ε between the PC chains, so the entropy-driven conformational freedom dominates over the energy-driven local properties [23], which means that attractive interactions do not play an important role for PC dynamics [24].

With more time, more attention was given to the dynamic properties of coarse-grained PC, exploring the center-of-mass diffusion, diffusion of PC segments, the mapping to realistic times, and the entanglement length [25,26]. This was made possible by important contributions of Hahn *et al.* [27] and Meyer *et al.* [28], who thoroughly designed an atomistic PC model, and Abrams *et al.* [29], who, based on the improved atomistic model, developed a coarse-grained model which employs four beads per monomer although it still includes a purely repulsive nonbonded potential. The details of the nonbonded interactions, however, in particular attractions become quite relevant the closer the system is to the glass transition.

As for the glass transition temperature T_g of PC, it has already been, to reasonable agreement, reproduced for short chains (21 monomers) in all-atom MD simulations by Fan *et al.* [30]. To the best of our knowledge, though, there have been no coarse-grained PC models published yet that reproduced T_g or the density as a function of temperature, respectively, from which T_g can be determined. This is again due to the difficulty of parameterizing all possible interactions among three different functional groups (the phenyl group occurs twice per monomer). Recently, this has been accomplished through the iterative Boltzmann inversion method, but due to the difficulty of sampling a statistically relevant amount of atomistic conformations at lower temperatures, the temperature at which the potentials have been calculated ($T = 480$ K) is too far beyond the glass transition [31]. At these temperatures, the shapes of the potential functions include complicated, nonlinearly temperature-dependent entropic contributions (from entanglement, e.g.) and thus are not generally transferable to different state points [32].

In the case of simpler polymers, consisting of only one type of bead (bead-spring model), experimental glass transition temperatures have indeed been reproduced with the help of a T-dependent potential scaling factor applied to potentials derived by the iterative Boltzmann inversion method [33,34]. The glass transition has also been quite accurately simulated in the case of polystyrene, using an attractive Lennard-Jones potential [35], and polyethylene, employing a similar potential but with the exponents 9 and 6 instead of 12 and 6 [36].

In the present study, we propose a coarse-grained potential for PC which respects the Hamaker far-field behavior [37] and is different from all previously published potentials that have been applied to coarse-grained polymers. The potential is fitted to the temperature-dependent density (or specific volume) from experiments using only two fit parameters which share the same value across all bead-bead interactions. Due to the low number of free parameters, the correct fits are quickly obtained, and despite the low number of free parameters, our model is the first coarse-grained model that reproduces molecular-weight-dependent experimental glass transition temperatures, the thermal expansion behavior, and several elastic properties of PC with surprising accuracy. The insights gained through our model will help us to better link experimentally accessible macroscopic properties of PC to the molecular-scale behavior of the PC chains, which would ultimately allow us to predict physical properties for entirely new materials using an automated simulation workflow.

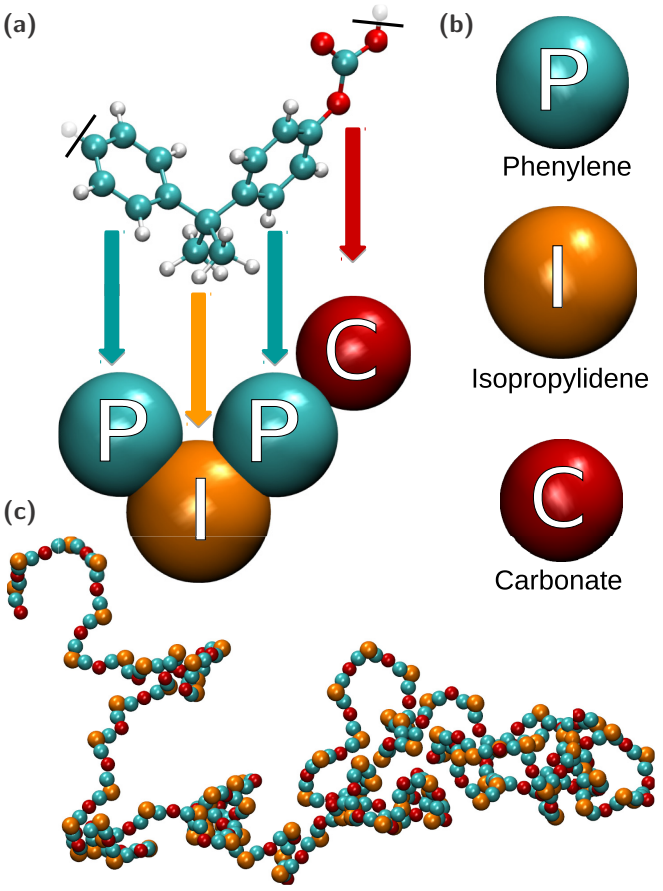

FIG. 1. Illustration of the coarse-grained polycarbonate (PC) model. The PC monomer (a) is divided in two phenylene groups, one isopropylidene group, and one carbonate group. Each group is substituted by a bead (b). The coarse-grained monomers are connected to form a linear polymer chain (c). The bonds and angles in the chain are governed by an intramolecular force field developed by Choudhury *et al.* [31].

II. METHODS

A. Simulation model

A PC monomer consists of two phenylene groups, one isopropylidene group, and one carbonate group, all linearly connected with each other [Fig. 1(a)]. The choice of our model is directed by our desire to reproduce key physical properties of PC in the most pragmatic way possible. Therefore, we employ a coarse-graining procedure as illustrated in Fig. 1. In order to create a coarse-grained model, each group is mapped onto a bead [P, I, or C; see Fig. 1(b)]. Monomers (P-I-P-C) can be connected to form chains of any desired length [Fig. 1(c)]. Each chain is terminated by a P bead on one end and a C bead on the other.

The coarse-grained simulations are performed using the GROMACS package (version 5.0.7) for MD simulations [38]. The beads are interacting with each other through a classical force field. The underlying equation solved in our simulations is Newton's equation of motion with an added stochastic thermostat (required to simulate an *NVT*, i.e. canonical, ensemble) and a barostat (required for an *NPT*, i.e. isothermal-isobaric, ensemble). The equation of motion is solved using a leapfrog algorithm with a time step Δt_s which corresponds to 10 times the smallest oscillation period in our system, i.e., the oscillation of the bond between the I and the P beads. That means for our simulations that $\Delta t_s = 3 \times 10^{-3}$ ps.

The potential energy in the system consists of intramolecular interactions between bonded coarse-grained beads and intermolecular interactions between nonbonded beads. The bonded interactions are describing (i) the distances between neighboring beads, (ii) the angles between consecutive bonds, and (iii) the torsional angles between the next but one bonds. All intramolecular interactions were kindly provided to us by Choudhury *et al.*, who determined them using the iterative Boltzmann inversion method [31]. Because of their nonanalytical nature, we implement them into our simulations in the form of tabulated values. With permission from Choudhury *et al.* [31], we also include the tables in the Supplemental Material [39].

As for the intermolecular interactions, we derived a pair potential from a far-field Taylor expansion of the Hamaker interaction [37] between two spheres i, j of equal and non-negligible diameters σ_{ij} in a distance r_{ij}. This potential has the functional form [19]

$$V(r_{ij}) = A\left(\frac{F\sigma_{ij}}{r_{ij}}\right)^{10} - B\left(\frac{F\sigma_{ij}}{r_{ij}}\right)^{8} - C\left(\frac{F\sigma_{ij}}{r_{ij}}\right)^{6}, \quad (1)$$

where i, j denote the types of the beads involved (i.e., phenylene, isopropylidene, or carbonate). By means of approximation, if $\sigma_{ii} \neq \sigma_{jj}$, then the Lorentz-Berthelot mixing rules yield $\sigma_{ij} = (\sigma_{ii} + \sigma_{jj})/2$. In our work, we refer to this potential as *10-8-6 potential*. The coefficient C, which is scaling the r^6 long-range interaction, originates from the expansion of the Hamaker interaction in the limit $r_{ij} \to \infty$. It is related to the Hamaker constant $\mathcal{H}$ of PC via $C = \mathcal{H}/36$. The value of $\mathcal{H} = 4\pi^2\tau^2\varepsilon_{\mathrm{av}}\sigma_{\mathrm{av}}^6 = 66$ kJ/mol is calculated from the atomic-weight-weighted Lennard-Jones parameters $\sigma_{\mathrm{av}} = 0.35$ nm and $\varepsilon_{\mathrm{av}} = 0.3$ kJ/mol of the atomistic PC in accordance with the GAFF force field [40] in addition to the atomic-weight-weighted number density $\tau = 57\,\mathrm{nm}^{-3}$ at room temperature. The coefficient A guarantees that V satisfies the condition $V(\sigma_{ij}) = 0$, from which follows that $A = B + C$. Finally, the coefficient B is used as a free parameter for scaling the depth of the potential in order to fit our model to experimental values.

The effective bead diameters σ_{ii} were first obtained from fitting Eq. (1) to the effective intermolecular pair potentials provided to us by Choudhury *et al.* [31]. However, due to the height of the temperature at which those coarse-grained potentials were developed, the extracted σ_{ii} values are too high for use in the temperature range that is relevant for this work. Especially the effective phenylene bead diameter is overestimated. Therefore, we exchange the phenylene bead diameter with one obtained from a *steered molecular dynamics* calculation of the potential of mean force (PMF) between two benzene rings in vacuum at $T = 420$ K (using a stochastic thermostat) [41]. Thus, our bead diameters are $\sigma_{\mathrm{PP}} = 0.464$ nm, $\sigma_{\mathrm{II}} = 0.5455$ nm, and $\sigma_{\mathrm{CC}} = 0.414$ nm. Finally, all σ_{ij} are multiplied by a uniform scaling factor F which is used as the second free parameter of the 10-8-6 potential.

We note that the atomistic Hamaker constant defines us an effective $\widetilde{\varepsilon}_{\mathrm{av}}$, which has, according to the far-field expansion of the Hamaker interaction, the value $\widetilde{\varepsilon}_{\mathrm{av}} = \mathcal{H}/144$. With this, as well as with $\widetilde{\tau} = 11.5\ \mathrm{nm}^{-3}$ and the average of our final (see Sec. II C) bead sizes $F\widetilde{\sigma}_{\mathrm{av}} = 0.455$ nm, we can determine the Hamaker constant of our model to be $\mathcal{H}_{\mathrm{CG}} = 21$ kJ/mol. Our result compares well with chemically similar polymer materials at similar operating conditions [42,43].

To summarize, the free parameter B scales the depth of the 10-8-6 potential, and the free parameter F scales the bead diameters. We will show that these two factors, which do not depend on the bead type, are all we need to reproduce many physical properties of PC.

B. Calculation of the glass transition temperature

Our system consists of linear coarse-grained PC chains, each composed of 100 monomers (i.e., P-I-P-C subunits). This is a typical length for PC in industrial applications, as it ensures a high degree of entanglement [25], which is required for elastic materials and durable products. The size of the system, i.e., the total number of chains in our simulation, is limited by finite-size effects on the one hand, introduced by periodic boundary conditions, and the necessary computation time on the other hand. By testing the thermal expansion behavior in systems of different sizes, we have found the minimum size at which finite-size effects become negligible: The optimal system size is 6000 beads or 15 chains with 100 monomers each [see snapshot in Fig. 2(a)]. We also perform a few simulations with 100 chains, in order to increase the statistical accuracy of our final results. The tabulated bead-bead interactions are cut off at a distance of 1.75 nm. The temperature and pressure are controlled by a velocity-rescaling thermostat and a Berendsen barostat, respectively.

In the initial configurations, the PC chains are supposed to be entangled with each other. The initial configurations are prepared at 1 bar external pressure according to the following recipe (the corresponding scripts are included in the Supplemental Material [39]):

(1) A single PC chain is equilibrated at an artificially high temperature (3000 K) in an *NVT* ensemble without periodic boundary conditions. Due to the decrease of the persistence length l_p of the chain to less than the order of one monomer, the chain equilibrates to a swollen but extremely wiggly structure, similar to Fig. 1(c).

(2) Fifteen copies of the equilibrated chain are put at random positions and with random orientations into a simulation box for an *NPT* ensemble simulation.

(3) With the barostat set to 1 bar, the temperature of the system is gradually decreased from 3000 to 900 K. Due to the vigorous thermal motion and the random initial orientations, the swollen, wiggly PC chains easily entangle with their partners.

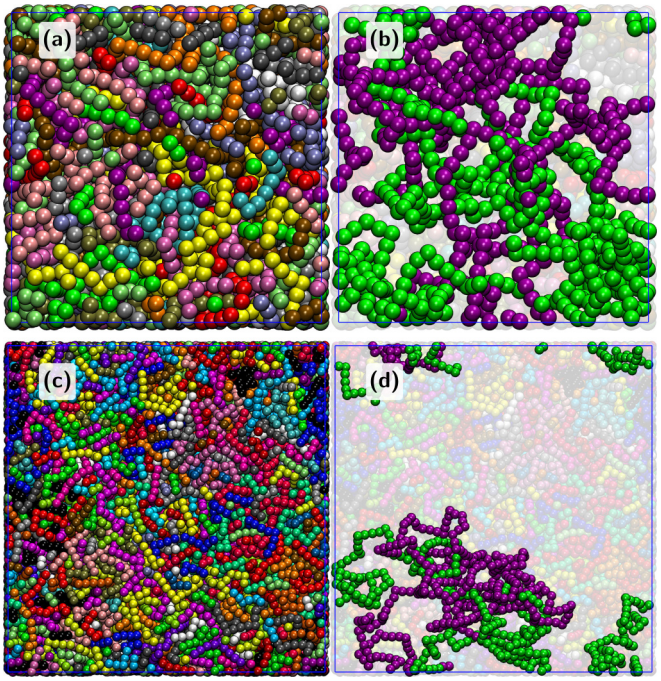

FIG. 2. Simulation snapshots of the glassy state at $T = 200$ K. Each PC chain has a unique color. (a) A *small* system consisting of 15 chains with length $N = 100$ each. (b) Two exemplary entangled chains taken from the small system. (c) A *large* system of 100 chains with length $N = 100$ each. (d) Two exemplary entangled chains taken from the large system. The small system (a) is used during the force field parametrization in Sec. II C and for the calculation of the elastic properties in Sec. III D. The large system (b) is used to determine the glass transition temperature T_g and the volume expansion behavior V_s in Sec. III A. The total size (in terms of total number of beads) of the systems used to simulate the molecular weight dependence of V_s and T_g in Sec. III B and III C is the same as in panel (a).

With the new initial configuration, the glass transition temperature is obtained in analogy to a dilatometry experiment. We apply the simulated annealing algorithm starting with 900 K and gradually cooling down to 200 K. The cooling rate is provided and discussed in the Supplemental Material [39]. The thermodynamic states sampled between $T = 600$ K and $T = 900$ K are not relevant for our analysis per se, but the high thermal energies in the beginning of the simulations help to equilibrate the structures before the chain dynamics become too slow. The dependence of T_g on the cooling rate Γ has been discussed for polymers in several studies [44,45].

After the simulation, the change of the specific volume $V_s(T) = 1/\rho(T)$ of the system is calculated as a function of temperature. Typically, $V_s(T)$ should have two regimes characterized by different volume expansion coefficients. Each regime can be fitted by a linear function. The transition between the regimes corresponds to the glass transition. The glass transition temperature T_g is defined as the temperature at the intersection of the linear fits [2,33,35,36].

C. Fitting of the potential

We fit the free parameters of Eq. (1) to reproduce experimental $V_s(T)$ results published by Zoller *et al.* [9]. We use

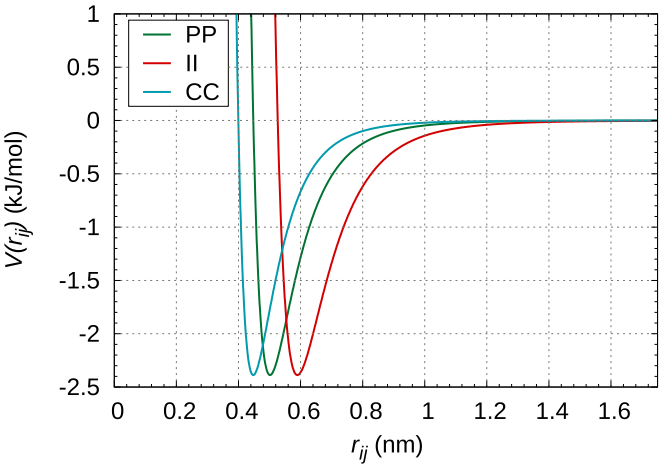

FIG. 3. The intermolecular potentials [Eq. (1)] of phenylene (P), isopropylidene (I), and carbonate (C) after fitting. The final fit parameters are $B = 25$ kJ/mol and $F = 0.965$. The mixed-bead potentials obey the Lorentz-Berthelot mixing rules.

only two fit parameters: The free parameter B scales the depth of the 10-8-6 potential and the free parameter F scales the bead diameters σ_{ij}. Our only goal is to find a set (B,F) for which our model reproduces the experimental glass transition temperature T_g and the specific volume at $T = 300$ K, V_s (300 K). As we will see, though, the model will reproduce much more than that.

As a first orientation, we qualitatively analyze the sensitivity of T_g and V_s (300 K) to changes of B and F within their individual reasonable value range. It turns out that T_g is much more sensitive to changes of B than of F. On the other side, V_s (300 K) is more sensitive to changes of F than of B. Based on this information, we iterate B and F as follows:

(1) The σ_{ij} values are set to default and F is set to 1. Parameter B is altered until the target $T_g = 422$ K is reached.

(2) After that, F is changed until $V_s(300\,\mathrm{K}) = 0.837$ g/cm^3.

(3) Next, since T_g has slightly changed with F, B is fine-tuned to get the right T_g again.

(4) The latest step has slightly changed V_s (300 K), so F is fine-tuned to obtain the correct V_s (300 K) value.

After iterating steps 3 and 4 a few times, we converge to $B = 25$ kJ/mol and $F = 0.965$, for which we obtain $T_g = 426$ K and $V_s(300\,\mathrm{K}) = 0.838$ g/cm^3. These results lie well within the spread of experimentally measured PC glass transitions. The corresponding 10-8-6 potentials are plotted in Fig. 3 for the PP, II, and CC interactions. Since A, B, and C are bead independent, all potentials have the same depth of $V_{\min} = -2.39$ kJ/mol. The mixed-bead potentials have all the same depth, while the effective bead sizes obey the Lorentz-Berthelot mixing rule.

III. RESULTS AND DISCUSSION

A. Glass transition and thermal expansion behavior

Now that the fit parameters B and F are fixed, we simulate the glass transition one more time, but with 100 chains instead of 15, to increase the statistical accuracy [see snapshot in

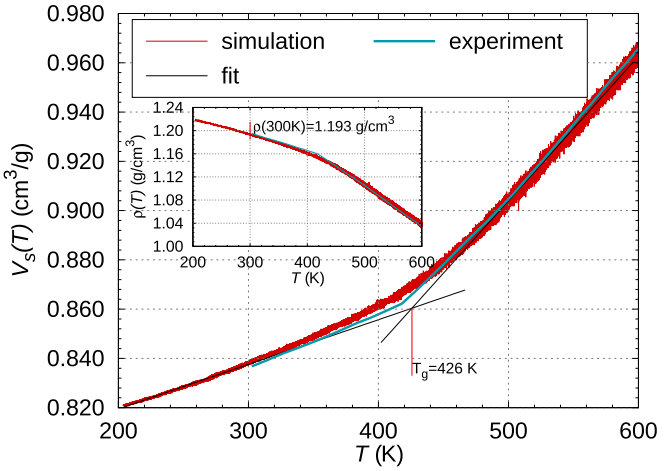

FIG. 4. The thermal expansion characteristic of PC from a simulation of 100 chains of 100 monomers each at 1 bar pressure. The glass transition temperature T_g is defined as the intersection of the linear fits of the thermal expansion curve. Inset: the temperature-dependent density $\rho(T) = (V_s(T))^{-1}$. The experimental values are from Zoller *et al.* [9].

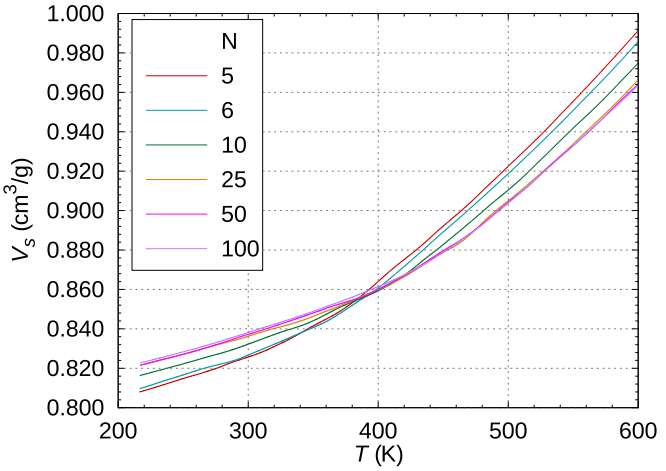

FIG. 5. The thermal expansion characteristic of PC at 1 bar pressure for different chain lengths N.

Fig. 2(c)]. The simulation can be recreated with the files included in the Supplemental Material [39]. The resulting $V_s(T)$ relationship is presented in Fig. 4 and compared to measurements from Zoller *et al.* [9]. For future reference, note that the specific volume reported by Zoller *et al.* is very similar (within less than $\pm 0.25\%$ deviation) to data provided by Mitsubishi Engineering Plastics [5] or data from Mercier *et al.* [7] Both temperature regimes in Fig. 4, $T < T_g$ and $T > T_g$, are again fitted each by a linear function. Since both sides of the simulated $V_s(T)$ curve slightly deviate from linearity, the results of the fitting are sensitive to the choice of the specific temperature range of each fit. This behavior translates into an error for the glass transition temperature of $\Delta T_g \pm 5$ K and for the volume expansion of $\Delta dV_s/dT = \pm 2 \times 10^{-5}$ (cm^3/gK). As it turns out (see Table I), not only do the glass transition temperature T_g and the specific volume $V_s(300\,\mathrm{K})$ agree considerably well with experiments, but also the volume expansion dV_s/dT in both the glassy ($T < T_g$) and fluid ($T > T_g$) state is recreated by our model with a deviation from the experimental values of less than 20%. Consequently, the correct specific volume (or the corresponding density $\rho(T) = [V_s(T)]^{-1}$ as shown in the inset of Fig. 4) is well reproduced over the entire considered temperature range.

B. Molecular weight dependence of the specific volume

Of enormous interest for industrial applications is the relationship between the molecular weight of a polymer (i.e., degree of polymerization N or chain length) and the glass transition temperature. The simulations are prepared according to the algorithm presented in Sec. II B. Note that the systems are all monodisperse. We have included all input files necessary to recreate these simulations in the Supplemental Material [39]. In Fig. 5, we demonstrate the thermal expansion curves for chains of different length, starting with $N = 5$ monomers, which is in the order of the polymer's persistence length. This marks the lowest value interesting for industrial applications, since shorter chains do no longer entangle, resulting in very brittle materials. We do not go beyond $N = 100$, since the corresponding entanglement is sufficient for most applications (if not even saturated) and there is no gain from even longer polymers but rather an unnecessary increase in computational cost.

Several interesting trends can be observed in Fig. 5 and the corresponding Table II: First, at $T > T_g(N)$ the specific volume decreases with increasing N, $(dV_s/dN|_{T>T_g} < 0)$. Second, $T_g(N)$ increases with N. Third, at $T < T_g(N)$ the specific volume increases with N, $(dV_s/dN|_{T<T_g} > 0)$. Fourth, far from $T_g(N)$ the thermal volume expansion dV_s/dT seems not to depend on N.

The ambidextrous behavior of $dV_s(N)/dN$ can be explained by different effects that dominate at different temperatures. At high T, the specific volume is determined by the ranges of the attractive bead-bead interactions. A decrease of N increases the fraction (i.e., concentration) $\mathcal{N}_{\mathrm{ter}}/\mathcal{N}_{\mathrm{tot}}$ of terminal beads ($\mathcal{N}_{\mathrm{ter}}$) relative to the total number of beads ($\mathcal{N}_{\mathrm{tot}} = 4N$). When that happens, bonded interactions are replaced by LJ interactions. Since the minima of the LJ interactions are located at higher bead-bead distances than the minima of the bonded

TABLE I. Results obtained from the thermal expansion characteristic of PC corresponding to Fig. 4. We compare the glass transition temperature T_g, the specific volume at room temperature $V_s(300\,\mathrm{K})$, and the volume expansion dV_s/dT below and above T_g to experiments [9].

	T_g (K)	V_s (300 K) (cm^3/g)	$\frac{dV_s}{dT}\|_{T<T_g}$	$\frac{dV_s}{dT}\|_{T<T_g}$ (cm^3/gK)
Simulation	426 ± 5	0.838	$1.8 \pm 0.2 \times 10^{-4}$	$5.9 \pm 0.2 \times 10^{-4}$
Experiment [9]	422	0.837	2.2×10^{-4}	6.1×10^{-4}

TABLE II. Results obtained from the thermal expansion characteristics of PC corresponding to Fig. 5. We compare the glass transition temperature T_g, the volume expansion dV_s/dT below and above T_g, and the density ρ at room temperature for (monodisperse) systems consisting of chains of different length N.

N	T_g (K)	$\frac{dV_s}{dT}\|_{T<T_g}$	$\frac{dV_s}{dT}\|_{T>T_g}$ (10^{-4} cm^3/(gK))	ρ (g/cm^3)
5	351	2.0	5.8	1.211
6	364	2.0	5.8	1.210
10	384	1.8	5.5	1.202
25	414	1.8	5.7	1.196
50	423	1.9	5.7	1.194
100	426	1.8	5.9	1.193

interactions, a decrease of N increases the specific volume and vice versa.

While T decreases, the shorter chains not only have more space for moving, but due to the lower number of constraints per molecule they are also more mobile than longer chains. Both effects contribute to the lowering of the corresponding T_g.

When T passes T_g, the polymers turn into a sterically arrested, nonequilibrium state. A major N-dependent contribution to the specific volume of the system is then the remaining unoccupied space between the entangled chains, the so-called void volume. In simple terms, as longer chains need more time to equilibrate than shorter chains, for sterical reasons, the former leave more void volume during the glassification than the latter [4].

In addition, we plot in Fig. 6 the specific volume as a function of the chain length at fixed temperatures [Fig. 6(a), $T = 300$ K; Fig. 6(b), $T = 500$ K]. In accordance with Fox and Loshaek [3], the specific volume can be fitted by

$$V_s(N) = V_s(\infty) - \frac{V_s(\infty) - V_s(1)}{N}, \tag{2}$$

where $V_s(\infty)$ and $V_s(1)$ are the limiting values for systems consisting of infinitely long polymers or just monomers, respectively. The concentration of terminal beads in the system is related to the degree of polymerization via $2\mathcal{N}_{\text{ter}}/\mathcal{N}_{\text{tot}} = 1/N$. Thus, Eq. (2) can be rewritten as

$$V_s(N) = V_s(\infty) - 2[V_s(\infty) - V_s(1)]\frac{\mathcal{N}_{\text{ter}}}{\mathcal{N}_{\text{tot}}}. \tag{3}$$

This means that the specific volume linearly depends on the fraction (or concentration) of terminal beads in the system.

The standard deviation of V_s is three to five times as high at 500 K as it is at 300 K. This is qualitatively consistent with the increase in compressibility with temperature [46], since volume fluctuations and compressibility are related to each other via the fluctuation-dissipation theorem. For both temperatures, the fit lies well within the fluctuations of the volume. However, the standard error of the calculations is smaller than the points in the plot. So, the fact that our calculated values stray from the fit at 500 K indicates that our 10-8-6 potential becomes less reliable with rising temperature.

At $T = 500$ K, the specific volume V_s grows proportionally with the concentration of terminal beads [see insets of Fig. 6(b)] due to the higher emphasis on LJ interactions associated with them. By contrast, at $T = 300$ K an increase in terminal bead concentration contributes negatively to the specific volume. The volume decreases proportionally with increase of the terminal bead concentration, which is contradicting measurements of various other thermoplastics, which show an increase of V_s with increasing terminal bead concentration (i.e., with decreasing N) at all temperatures [3,36]. Even more so, we contradict measurements of PCs which also show an increase of V_s with the terminal bead concentration of one magnitude higher than our simulations over the whole temperature range [7]. It seems that our model strongly underestimates the contribution of the chain ends to the specific volume.

A possible explanation comes from experiments on polyethylene glycol (PEG) and polydimethyl siloxanes (PDMS) [47]. In the case of PEG, the specific volume only weakly depends on the chain length. As the terminal groups of PEG are allowed to form strong hydrogen bonds, the formation of these bonds reduces the number of DOF of the terminal groups to the extent that they exhibit properties similar to the main chain segments. On the other hand, the terminal

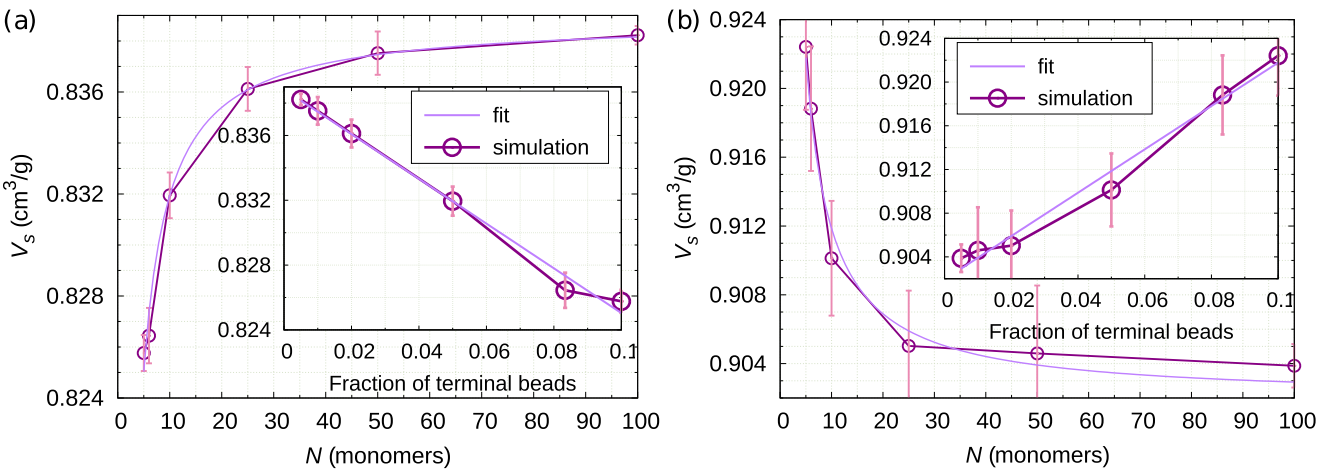

FIG. 6. The specific volume at $T = 300$ (a) and 500 K (b) as function of the degree of polymerization N. Insets: the corresponding specific volume as function of the ratio between the number of terminal beads in the simulation and the total number of beads, $\mathcal{N}_{\text{ter}}/\mathcal{N}_{\text{tot}}$.

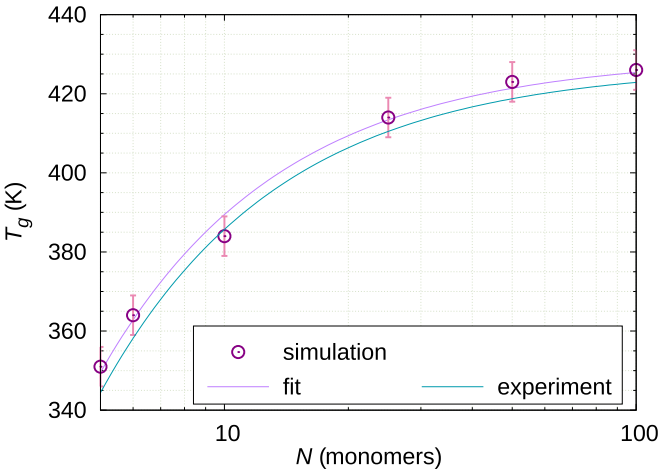

FIG. 7. The glass transition temperature as function of the degree of polymerization N. The simulated values are fitted using Eq. (4). The experimental values are from Mitsubishi Engineering Plastics [5].

groups of PDMS cannot form hydrogen bonds. Hence, they have more DOF which can contribute additional volume to the extent that the terminal beads dominate the dependence of V_s. Accordingly, a strong dependence of V_s on the chain length has been observed in experiments.

As for our case, the PCs from the corresponding reference studies (Lexan in the case of Mercier *et al.* [7]) are terminated by phenyl rings, which do not form hydrogen bonds. Our model is different from that in two respects. First, only half of our terminal beads represent phenyl rings. The other half is made up by carbonate beads, which differ but moderately from the phenyl beads in size. Second, we assume the same attractive nonbonded potential for the terminal beads as for the beads in the main chain. The second reason will be the crucial one, in case our terminal beads are too attractive. A solution for this conundrum is proposed in the following section.

C. Molecular weight dependence of the glass transition temperature

Interestingly, the molecular weight dependence of the glass transition temperature is not affected by the missing volume contribution, which is demonstrated in Fig. 7. For linear polymers, Fox *et al.* [2,3] discovered a relation between the glass transition temperature $T_g(N)$ and the inverse of the chain length N which has been repeatedly validated [48–50] and reads

$$T_g(N) = T_g(\infty) - \frac{K_g}{N}. \tag{4}$$

The quantity $T_g(\infty)$ is the glass transition temperature in the limit of infinitely long chains and K_g is an empirical constant. Our simulation results compare very well to measurements published by Mitsubishi Engineering Plastics [5]. The reported values for the coefficients of Eq. (4) are (in units used in this paper) $T_g^{\mathrm{exp}}(\infty) = 427$ K and $K_g^{\mathrm{exp}} = 412.9$ K. With a small overestimation of less than 5 K on average, a fit of Eq. (4) to our simulation results yields $T_g^{\mathrm{sim}}(\infty) = 429.4 \pm 2.0$ K and $K_g^{\mathrm{sim}} = 399.2 \pm 16.9$ K. Unfortunately, the dependence of the specific volume on the chain length is not published by Mitsubishi Engineering Plastics. Alternative experimental values for the coefficients of Eq. (4) reported in literature are given in Table III. Yet other studies used theories different from Eq. (4) to express $T_g(N)$ [11,51]. All of these studies have in common that they report significantly stronger N dependencies of the glass transition temperature (such as higher K_g values) than Mitsubishi Engineering Plastics.

So, to retrace our steps taken in Secs. III B and III C before coming to a conclusion, we found out that the specific volume in our model changes linearly with the concentration of terminal beads, which agrees with experiments, but in contrast to experiments the dependency in our model is much weaker. However, experiments have shown that polymers such as PEG, which terminal groups can form hydrogen bonds, also have a weak chain length dependence of the specific volume. Next, our model very well reproduces the experimental chain length dependence of the glass transition temperature published by Mitsubishi Engineering Plastics [5]. However, there are other experimental studies on PC that report significantly stronger dependencies [7,8,11,51].

We do not know which chemical groups are terminating the PCs from Mitsubishi Engineering Plastics, but they may as well be phenols, which would al least qualitatively explain the relatively weak chain length dependence of the glass transition temperature due to hydrogen bonding. After all, the infrared absorption spectrum of the PC resins published by Mitsubishi Engineering Plastics [5] in their data sheets indeed hints, by means of a small corrugation at ≈3500 cm^{-1}, at the presence of at least some amount of −OH groups (but it could also be just some residual water in the analyzed samples). Also the rate of water absorption at room temperature, at a value of 0.23% after 24 h and 0.35% at saturation, is relatively high for PC resins. Unfortunately, we do not have sufficient decisive experimental data to come to a clear conclusion.

As for our model, the terminal beads interact attractively with all other beads. Even though the pair potentials in our

TABLE III. The coefficients for Eqs. (3) and (4), describe the dependence of the specific volume and of the glass transition temperature on the chain length.

	$T_g(\infty)$ (K)	K_g (K)	$V_s(\infty) - V_s(1)\vert_{300\mathrm{K}}$ (cm^3/g)	$V_s(\infty) - V_s(1)\vert_{500\mathrm{K}}$ (cm^3/g)
present study	429.4 ± 2.0	399.2 ± 16.9	0.069	−0.099
Mitsubishi E. P. [5]	427	412.9	–	–
Adam *et al.* [8]	432	570	–	–
Mercier *et al.* [7]	427	700	−0.4	−0.7

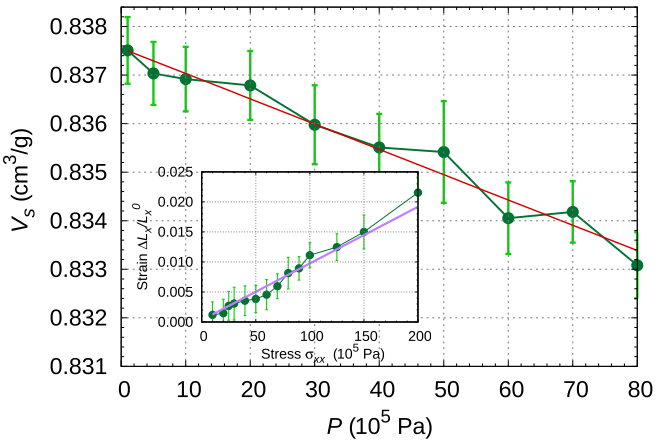

FIG. 8. The response of our PC model to external stresses at room temperature. The bulk modulus is calculated from the average slope of $V_s(P)$ (red line) via $K = -(d \ln V_s/dP)^{-1}$. The applied pressure P is isotropic. The inset shows the strain $\Delta L_x/L_x^0$ as the response to a uniaxially applied stress σ_{xx}. The Young's modulus E is the inverse of the average slope of the strain (purple line).

model are weak compared to hydrogen bonds, each bead can interact with multiple beads at a time. Ultimately, our model reproduces quantitatively the thermal expansion characteristic of long PCs ($N = 100$) and the N-dependent glass transition temperature of one particular PC. Qualitatively, our model reproduces the linear dependence of the specific volume on N in a way that is consistent with attractive chain ends.

D. Elastic properties

We finally analyze the response of our model to external stresses at room temperature $T = 300$ K in order to compare our model's bulk modulus K, Young's modulus E, and Poisson ratio ν to the real case. To calculate the bulk modulus $K = -(\frac{d \ln V_s}{dP})^{-1}$ (at constant T), we couple a previously at $T = 300$ K and $P = 1$ bar equilibrated configuration of the 15-chain system to different isotropic pressures P in the range of 1 to 80 bar. As for the Young's modulus, we assume that it is isotropic for randomly coiled and oriented polymers, and so the system is coupled to different uniaxial stresses σ_{xx}, while σ_{yy} and σ_{zz} are kept at 1 bar. Measuring the resulting deformation ΔL_x of the box length in x direction from the original 1-bar length L_x^0 enables us to use Hooke's law $\sigma_{xx} = E\Delta L_x/L_x^0$ to calculate the Young's modulus E. Finally, the Poisson ratio is obtained from the relation $\nu = \frac{1}{2}(1 - \frac{E}{3K})$. The results are plotted in Fig. 8. The red lines are linear fits representing the averages of the results. The slope of the $V_s(P)$ fit reveals a value for the bulk modulus of $K = 1.6 \times 10^9$ Pa. The slope of the linear regime [52,53] of the stress-strain relation yields values for the Young's modulus which average to $E = 1.06 \times 10^9$ Pa. The corresponding Poisson ratio is $\nu = 0.39$. The standard deviations of the specific volume at constant pressures have the same magnitude as the standard deviations at constant $T = 300$ K from Sec. III B. The high scatter around the linear fit is attributed to a lack of sampling, particularly in regard to the long equilibration time scales required to minimize the void volume at $T < T_g$.

Comparing our results to experimental values is difficult, as PC samples are produced industrially with partly undisclosed chemical additives and modifications. Measurements of entirely pure, monodisperse PC resins are, to our knowledge, not available. Material supplier Mitsubishi Engineering Plastics [5], for instance, provides resins with elastic properties in the range of $E = 1.7 \ldots 1.9 \times 10^9$ Pa, $K = 2.36 \ldots 2.64 \times 10^9$ Pa, and $\nu = 0.38$. Professional Plastics Inc. [54] lists values of $E = 2.3 \ldots 2.4 \times 10^9$ Pa, $K = 2.95 \ldots 3.08 \times 10^9$ Pa, and $\nu = 0.37$ for their products. More values can be found in Gilmour *et al.* [55] and Siviour *et al.* [53]. Our simulations underestimate both E and K by at least 50%, but we succeed in reproducing the correct Poisson ratio since E and K are underestimated in equal measure. The deviation from the real systems may be at least partly due to the lack of additives in our model or the lack of polydispersity.

IV. CONCLUSIONS

In summary, the goal of this work was to develop and test a very simple, yet efficient (in terms of computational cost and physical detail), coarse-grained MD model for the thermoplastic bisphenol-A polycarbonate. We use a bead-spring model, which we fit a very simple attractive potential function to, that is derived from the fundamental Hamaker theory. Although we are able present many of the strengths of our coarse-grained model, our procedure has limitations, too. Typically, an atomistic model is used to parametrize the coarse-grained model via the time-consuming iterative Boltzmann sampling, which ensures that the local intermolecular structure is conserved. A weak point of our particular procedure is the lack of an atomistic model counterpart to our coarse-grained model. As a consequence, we are not necessarily able to reproduce the local intermolecular structure (e.g., in terms of the radial distribution function). Coarse graining also drastically reduces the number of degrees of freedom of the system, which could make it difficult to calculate realistic heat capacities. Furthermore, our 10-8-6 potential is independent of temperature. This means that we implicitly integrate into our potential the entropic contributions that play a role in the glass transition only.

Yet, our model is the first that reproduces many physical PC properties that are critical from a manufacturing standpoint: This is mainly the glass transition temperature and the associated volume expansion behavior, as well as—to a lesser extent—elastic properties. Considering how heavily coarse grained our model is, our results for the bulk modulus, the Young's modulus, and especially for the Poisson ratio are remarkably close to the experimental values. Most importantly, we find that despite its simplicity, our model reproduces not only the glass transition temperature correctly but also the specific volume (or density) over a high temperature range ($200 < T < 600$ K). To further validate our model, we analyze the volume expansion behavior for (perfectly monodisperse) systems of different molecular weight. In particular, at constant T, we find a linear dependence of the specific volume with the concentration of terminal beads. With the chain length comes also a change in the temperature at which the glass transition occurs. Here, our simulations are in very good agreement with experiments on one particular type of PC. However, regarding

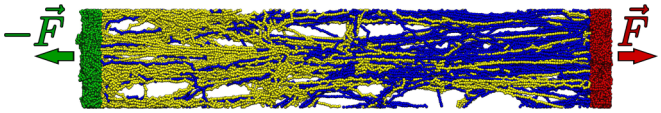

FIG. 9. Preliminary simulation (snapshot) of the tensile response (tensile strength, rupture energy, entanglement, etc.) to stretching two sides of a PC sample until it ruptures, similar to Ref. [56]. The PC beads marked with green and red colors are being pulled at with a constant force in opposite directions. The yellow chains are those which are connected to the green beads, and the blue chains belong to the red beads.

experiments, the polydispersity of the material, the chemistry of the chain ends, or the presence of chemical additives usually are unknown variables not provided by the PC manufacturers. For that reason it is very difficult to correlate the volume expansion behavior, the glass transition temperature, and the molecular chain length with each other. Based on additional experimental data of non-PC materials, we can say that the dependence of T_g and V_s on N is qualitatively consistent with polymers that contain attractive terminal groups (by means of hydrogen bonds, e.g.). A decisive evidence (either for or against) would be a measurement of the OH concentration within the material that compares best to our model. This could be done by spectral analysis or water solubility measurements, for instance, which is beyond the scope of this work.

As it stands, we have presented a workflow for the theoretical prediction of polymer properties. We have demonstrated an expeditious approach to parameterizing a surprisingly powerful and speedy coarse-grained polymer model. The transition from an atomistic model to a coarse-grained one entails the reduction of (a) the fastest vibration frequencies, (b) the number of numeric calculations, and (c) the number of degrees of freedom. In combination, these three factors increase the simulation speed by one to three orders of magnitude compared to atomistic simulations, depending strongly on the chain length [31]. The model's capabilities have been ascertained by means of important static physical properties of monodisperse systems and they will be further advanced by studying polydispersity and mechanical properties.

An already realizable material application is lamination and delamination, as illustrated in Fig. 9. We can calculate the work required to rupture a PC bulk sample and the energy released by the creation of an interface. This is especially relevant in the context of the chain length to T_g relation, since many industrial applications require a good compromise between the processing temperature (i.e., energy cost) and material strength. Future work will also focus on dynamic properties such as self-diffusion, viscosity, or heat conductivity by way of which the model will be continuously improved until we will be able to correctly reproduce properties of structurally modified or functionalized PC molecules.

ACKNOWLEDGMENT

We wish to thank Chandan Kumar Choudhury (Clemson University, Clemson, SC, USA) for providing the intramolecular PC potentials used in this study and for the intermolecular PC potentials that we used to determine the initial values for our bead diameters.

[1] J. Bendler, *Handbook of Polycarbonate Science and Technology*, Plastics Engineering Series (Taylor & Francis, Philadelphia, 1999).
[2] T. G. Fox and P. J. Flory, J. Appl. Phys. **21**, 581 (1950).
[3] T. G. Fox and S. Loshaek, J. Polym. Sci. **15**, 371 (1955).
[4] G. Kanig, Kolloid. Z. Z. Polym. **190**, 1 (1963).
[5] Mitsubishi Engineering-Plastics Corporation, http://www.m-ep.co.jp/en.
[6] R. P. White and J. E. G. Lipson, ACS Macro Lett. **4**, 588 (2015).
[7] J. P. Mercier, J. J. Aklonis, M. Litt, and A. V. Tobolsky, J. Appl. Polym. Sci. **9**, 447 (1965).
[8] G. Adam, J. Hay, I. Parsons, and R. Haward, Polymer **17**, 51 (1976).
[9] P. Zoller, J. Polym. Sci. B Polym. Phys. **20**, 1453 (1982).
[10] E. Macho, A. Alegría, and J. Colmenero, Polym. Eng. Sci. **27**, 810 (1987).
[11] Z. Dobkowski, Eur. Polym. J. **18**, 563 (1982).
[12] G. D. Wignall and G. W. Longman, J. Mater. Sci. **8**, 1439 (1973).
[13] L. Červinka, E. Fischer, K. Hahn, B.-Z. Jiang, G. Hellmann, and K.-J. Kuhn, Polymer **28**, 1287 (1987).
[14] S. Tsai, I. Lan, and C. Chen, Comput. Theor. Polym. Sci. **8**, 283 (1998).
[15] J. H. Shih and C. L. Chen, Macromolecules **28**, 4509 (1995).
[16] H. Sun, S. J. Mumby, J. R. Maple, and A. T. Hagler, J. Am. Chem. Soc. **116**, 2978 (1994).
[17] C. F. Fan, T. Cagin, Z. M. Chen, and K. A. Smith, Macromolecules **27**, 2383 (1994).
[18] J. Baschnagel, K. Binder, W. Paul, M. Laso, U. W. Suter, I. Batoulis, W. Jilge, and T. Bürger, J. Chem. Phys. **95**, 6014 (1991).
[19] F. Müller-Plathe, Chem. Phys. Chem. **3**, 754 (2002).
[20] D. Reith, M. Pütz, and F. Müller-Plathe, J. Comput. Chem. **24**, 1624 (2003).
[21] K. M. Zimmer, A. Linke, D. W. Heermann, J. Batoulis, and T. Bürger, Macromol. Theory Simul. **5**, 1065 (1996).
[22] W. Tschöp, K. Kremer, J. Batoulis, T. Bürger, and O. Hahn, Acta Polym. **49**, 61 (1998).
[23] W. Tschöp, K. Kremer, O. Hahn, J. Batoulis, and T. Bürger, Acta Polym. **49**, 75 (1998).
[24] G. S. Grest, J. Chem. Phys. **145**, 141101 (2016).
[25] S. León, N. van der Vegt, L. Delle Site, and K. Kremer, Macromolecules **38**, 8078 (2005).
[26] B. Hess, S. León, N. van der Vegt, and K. Kremer, Soft Matter **2**, 409 (2006).
[27] O. Hahn, D. A. Mooney, F. Müller-Plathe, and K. Kremer, J. Chem. Phys. **111**, 6061 (1999).
[28] H. Meyer, O. Hahn, and F. Müller-Plathe, J. Phys. Chem. B **103**, 10591 (1999).
[29] C. F. Abrams and K. Kremer, Macromolecules **36**, 260 (2003).
[30] C. F. Fan, T. Çagin, W. Shi, and K. A. Smith, Macromol. Theory Simul. **6**, 83 (1997).

[31] C. K. Choudhury, P. Carbone, and S. Roy, Macromol. Theory Simul. **25**, 274 (2016).
[32] P. Carbone, H. A. K. Varzaneh, X. Chen, and F. Müller-Plathe, J. Chem. Phys. **128**, 064904 (2008).
[33] K. Prasitnok, J. Polym. Res. **23**, 139 (2016).
[34] K. Prasitnok and M. R. Wilson, Phys. Chem. Chem. Phys. **15**, 17093 (2013).
[35] H. Morita, K. Tanaka, T. Kajiyama, T. Nishi, and M. Doi, Macromolecules **39**, 6233 (2006).
[36] J. Zhao, S. Nagao, and Z. Zhang, J. Mater. Res. **25**, 537 (2010).
[37] H. Hamaker, Phys. (Amsterdam, Neth.) **4**, 1058 (1937).
[38] M. J. Abraham, T. Murtola, R. Schulz, S. Páll, J. C. Smith, B. Hess, and E. Lindahl, SoftwareX **1–2**, 19 (2015).
[39] See Supplemental Material at http://link.aps.org/supplemental/10.1103/PhysRevMaterials.1.043804 for details about the intramolecular potentials and simulation input files.
[40] J. Wang, R. M. Wolf, J. W. Caldwell, P. A. Kollman, and D. A. Case, J. Comput. Chem. **25**, 1157 (2004).
[41] S. Park, F. Khalili-Araghi, E. Tajkhorshid, and K. Schulten, J. Chem. Phys. **119**, 3559 (2003).
[42] R. H. French, J. Am. Ceram. Soc. **83**, 2117 (2000).
[43] H.-J. Jacobasch and K.-H. Freitag, Acta Polym. **30**, 453 (1979).
[44] R. Brüning and K. Samwer, Phys. Rev. B **46**, 11318 (1992).
[45] A. Soldera and N. Metatla, Phys. Rev. E **74**, 061803 (2006).
[46] T. Kikuchi, T. Takahashi, and K. Koyama, J. Macromol. Sci. B **42**, 1097 (2003).
[47] G. Dee, T. Ougizawa, and D. Walsh, Polymer **33**, 3462 (1992).
[48] S. Clarson, J. Semlyen, and K. Dodgson, Polymer **32**, 2823 (1991).
[49] R. París and J. L. De la Fuente, J. Polym. Sci. B Polym. Phys. **45**, 1845 (2007).
[50] K. Haraguchi and Y. Xu, Colloid Polym. Sci. **290**, 1627 (2012).
[51] R. Fedors, Polymer **20**, 518 (1979).
[52] J. G. A. van Houten, DCT rapporten, Eindhoven: Technische Universiteit Eindhoven (1994), see also: https://pure.tue.nl/ws/files/4402164/653970.pdf.
[53] C. Siviour, S. Walley, W. Proud, and J. Field, Polymer **46**, 12546 (2005).
[54] http://www.professionalplastics.com.
[55] I. W. Gilmour, A. Trainor, and R. N. Haward, J. Appl. Polym. Sci. **23**, 3129 (1979).
[56] T. Ge, G. S. Grest, and M. O. Robbins, Macromolecules **47**, 6982 (2014).